Title

Atomistic Investigations of the Effects of Si/Al Ratio and Al Distribution on the Adsorption Selectivity of n-Alkanes in Brønsted-Acid Zeolites

Journal

The Journal of Physical Chemistry C, 122(17)

ISSN

1932-7447

Authors

Yang, Chi-Ta
Janda, Amber
Bell, Alexis T
et al.

Publication Date

2018-05-03

DOI

10.1021/acs.jpcc.7b11190

Peer reviewed

THE JOURNAL OF PHYSICAL CHEMISTRY C

Article

Cite This: J. Phys. Chem. C 2018, 122, 9397−9410

pubs.acs.org/JPCC

Atomistic Investigations of the Effects of Si/Al Ratio and Al Distribution on the Adsorption Selectivity of *n*-Alkanes in Brønsted-Acid Zeolites

Chi-Ta Yang,[†] Amber Janda,[‡,§] Alexis T. Bell,[*,‡] and Li-Chiang Lin[*,†]

[†]William G. Lowrie Department of Chemical and Biomolecular Engineering, The Ohio State University, Columbus, Ohio 43210, United States

[‡]Department of Chemical and Biomolecular Engineering, University of California, Berkeley, Berkeley, California 94720, United States

Supporting Information

ABSTRACT: The adsorption of *n*-alkanes onto Brønsted-acid sites is a key step in the catalytic cracking of alkanes. Employing configurational-bias Monte Carlo simulations, we have investigated how the ratio of equilibrium adsorption constants for central C−C bonds relative to terminal bonds of *n*-alkanes (i.e., the adsorption selectivity ratio) in Brønsted-acid zeolites is influenced by the Si/Al ratio and the Al distribution. A new computational approach was implemented, and the developed force field was validated by a comprehensive comparison between simulation results and experimental data for a number of Brønsted-acid zeolites. While the adsorption selectivity seems to be relatively insensitive to the Si/Al ratio, our results reveal that the Al distribution plays a crucial role in determining the adsorption selectivity. Changes in the Al distribution result in a change of as much as 2-fold in the adsorption selectivity ratio for *n*-hexane. The selectivity generally shows larger variations with respect to Al distribution in zeolites with a larger Si/Al ratio. The two factors identified by this work that substantially influence the selectivity ratio are the siting of Al atoms among T-sites and their spatial proximity, and an atomic-level understanding of each of these effects was achieved. The siting of Al atoms at more or less selective T-sites significantly influences the overall selectivity ratio, and Al atoms in close proximity can synergistically enhance the adsorption of central C−C bonds, leading to a higher selectivity ratio relative to isolated Al atoms. We anticipate that these results will have important implications for future large-scale computational screenings and the development of advanced synthesis approaches to target certain Al distributions in zeolites.

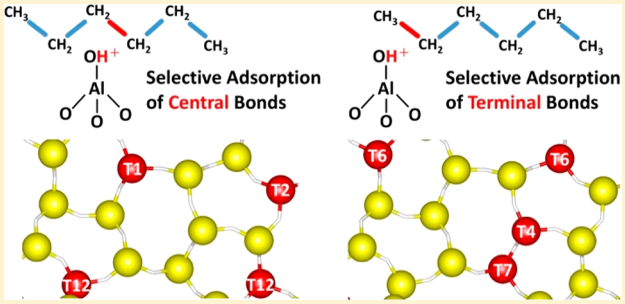

1. INTRODUCTION

In the past several decades, zeolites have been widely employed in many fields such as catalysis,[1] gas separation,[2] and ion exchange[3] due to a variety of desirable properties such as excellent thermal and chemical stability, large surface areas, and geometrically diverse topologies. Zeolites are crystalline, microporous materials consisting of corner-sharing $[AlO_4]^-$ and $[SiO_4]$ tetrahedra that form pores, cages, and/or channels of molecular dimensions. Brønsted-acid sites result when the negatively charged oxygen of $[AlO_4]^-$ is compensated by a proton. Such acidic zeolites are vital in petroleum refining,[4] petrochemicals production,[5] and pollution control,[6] and also catalyze the formation of 60−65% of the world's propylene via steam cracking and 30% through fluid catalytic cracking.[7]

Cracking of a C−C bond in an alkane at a zeolite Brønsted-acid site results in the formation of a smaller alkane and an alkene. This process can occur through both mono- and bimolecular mechanisms.[8,9] The monomolecular mechanism, involving the interaction of an alkane C−C or C−H bond with a Brønsted proton, dominates at conditions of low surface coverage (low pressure and conversion),[10] while the bimolecular mechanism, involving hydride transfer as well as oligomerization and beta scission of alkene intermediates,[11,12] primarily occurs under industrial conditions (high pressure, conversion, and surface coverage). Because of its simplicity and well-defined kinetics, the monomolecular alkane cracking, and also dehydrogenation, have been the subject of a number of studies aimed at elucidating the influence of zeolite structure on cracking kinetics.[13−21]

Adsorption thermodynamics play a crucial role in monomolecular cracking kinetics because the apparent rate coefficient is proportional to the equilibrium constant for alkane adsorption onto Brønsted protons and the intrinsic rate coefficient.[13,14,22−24] Measured activation parameters are consequently equal to the sum of the adsorption enthalpy and entropy and the intrinsic activation enthalpy and entropy, respectively.[22,23] To elucidate the influence of the adsorption equilibrium on apparent kinetics, and to extract intrinsic kinetic parameters, it is therefore necessary to obtain adsorption

Received: November 12, 2017
Published: January 3, 2018

DOI: 10.1021/acs.jpcc.7b11190
J. Phys. Chem. C 2018, 122, 9397−9410

thermodynamics of alkanes at protons (e.g., specific adsorption enthalpy and entropy, denoted respectively as $\Delta H_{ads\text{-}H+}$ and $\Delta S_{ads\text{-}H+}$; see Computational Method). We note that the adsorption of alkanes directly onto protons cannot be measured at reaction temperatures (>673 K), due to the tendency of the alkane to react and to locate increasingly at siliceous parts of the framework.[25−27,24] As a result, computational studies have been employed to access this information.[28,29]

Recently, we have developed an approach to calculate adsorption of alkanes at protons in zeolites[13] in which an efficient domain decomposition method was developed for use together with the Widom particle insertion method (described below). We also developed improved force field parameters,[13] fit to describe the interactions between the alkane and the proton, which moves rapidly among the O atoms of the negatively charged AlO_4^- groups at the temperature of cracking.[30,31] This methodology enabled us to systematically investigate the effects of zeolite pore and cage topology on the adsorption thermodynamics of *n*-alkanes adsorbed at Brønsted acid sites.[14] While a compensating effect of correlated changes in adsorption entropy and enthalpy on the free energy generally exists, it was found in our previous work that the adsorption free energy can be tuned by manipulating a characteristic dimension (e.g., changing the pore size) and topology (e.g., adding cages) simultaneously.[14] It is anticipated that this development can also facilitate the discovery of novel Brønsted-acid zeolites, serving as a powerful approach to discover zeolite candidates possessing desirable adsorption properties for alkane cracking. For example, by examining adsorption data reported in our recent theoretical work[14] together with selectivity data from our recent experimental work,[13] it can be seen that zeolites with higher selectivity to central C−C adsorption are also generally more intrinsically selective to central C−C cracking. Thus, an improved understanding of what zeolite properties influence the selectivity to adsorption of different C−C bonds of an alkane can serve as a guideline for the rational design of structures that are most likely to crack an alkane at a desired location.

Although significant progress has been made in understanding the influence of zeolite structure on alkane adsorption,[13,14] it is noted that these studies were performed for zeolites containing only isolated Brønsted protons. An atomic level understanding of the effects of the distributions of multiple Al atoms among different T-sites and channel environments, as well as of their proximity, is lacking. In this study, the adsorption properties of C4−C6 *n*-alkanes in Brønsted-acidic FAU, MOR, MFI, TON, FER, KFI, and MWW were investigated, using CBMC simulations in the Henry region,[18] which corresponds to the low coverages relevant to monomolecular cracking, as functions of the Si/Al ratio and Al distributions. Attention is focused on the selectivity ratio for adsorption via a central vs terminal C−C bond, which is expected to influence the selectivity for monomolecular alkane cracking. As noted above, it is expected that zeolites that are more selective to central C−C adsorption will generally also be more intrinsically selective to central C−C cracking.[13] Cracking at this location would be preferred in industrial applications such as the cracking of naphtha range alkanes to liquefied petroleum gas (LPG).

In the present study, the accuracy and transferability of the force field was first evaluated by comparing theoretical predictions with experimentally available measurements of $\Delta H_{ads\text{-}H+}$ and $\Delta S_{ads\text{-}H+}$ at room temperature in several Brønsted-acid zeolite frameworks having a range of Si/Al ratios. Next, the effects of the Si/Al ratio (ranging from 2 to 71) for adsorption of C4−C6 *n*-alkanes in a given zeolite framework was investigated for sets of 10 zeolite samples of the framework with random distributions of Al atoms. The role of the Al distribution in influencing the adsorption selectivity for a given framework at a constant Si/Al ratio was also studied. Notably, our results show that the selectivity toward adsorption via central C−C bonds can vary by as much as a factor of 2 as a function of the Al distribution among different T-sites. High selectivity to central C−C adsorption in 10 zeolite samples with randomly generated Al distributions was found to correlate strongly with the number of Al atoms located at T-site locations that exhibit high selectivity, while the range of the overall selectivity observed among samples correlated with the variation in selectivity among the individual T-sites. T-sites located in a more confined space appear to promote the adsorption of central C−C bonds. However, further study is needed in order to achieve a quantitative understanding of the effects of geometry on the selectivity ratio. The presence of nearby Al atoms (i.e., proximate Al atoms) was also found to affect the selectivity at a given T-site and increase the selectivity to central C−C adsorption. In order to gain atomistic understandings, insights into the enthalpy and entropy of adsorption are also discussed in the context of density maps that illustrate the distribution of configurations of the alkane near the proton.

Overall, the selectivity of alkanes for adsorbing via central vs terminal C−C bonds at Brønsted protons in zeolites is not generally constant for a given framework type, and exhibits more sample-to-sample variation for high Si/Al ratios and for more heterogeneous frameworks having a large range of the adsorption selectivity among individual T-sites. The results of this study provide a systematic understanding of the effects of the Si/Al ratio and the Al distribution on adsorption selectivity in zeolite materials, and facilitate the rational design of better zeolite catalysts to promote the cracking of central C−C bonds.

2. COMPUTATIONAL METHOD

Configurational-bias Monte Carlo (CBMC) simulations were used to compute the adsorption properties of linear alkanes (propane through *n*-hexane) in Brønsted-acid zeolites. Seven zeolites including MFI, TON, FER, MWW, MOR, KFI, and FAU were studied, chosen mainly on the basis of available experimental data.[32−35] The atomic structure of these zeolites was taken from the database of the International Zeolite Association (IZA).[36] In these calculations, to describe intermolecular and intramolecular interactions of alkanes, the TraPPE model,[37] a united atom approach, was adopted for representing methyl ($-CH_3$) and methylene ($-CH_2-$) groups of the alkanes. Nonbonded intermolecular interactions were described by Lennard-Jones 6−12 potentials, while appropriate potential functions were adopted to describe intramolecular interactions of bond stretching, bending, and torsion. To account for the interactions between linear alkane molecules and zeolite framework oxygen atoms, parameters developed by Dubbeldam et al.[38,39] for all-silica zeolites were used. The interaction between an alkane molecule and a Brønsted-acidic proton associated with the framework Al atom was described in our previous work;[13] an effective potential was developed for the interaction between the alkane and the oxygen atoms attached to Al atoms to account for the rapid relocation of the proton occurring at temperatures of cracking (>673 K).[30,31]

DOI: 10.1021/acs.jpcc.7b11190
J. Phys. Chem. C 2018, 122, 9397−9410

This parameter set was determined by fitting experimental data for *n*-alkane adsorption in Brønsted-acidic FAU (a structure that has 12-MR pores and large cages), using the experimental values of ΔH_{ads} (in contrast to the specific adsorption at protons, ΔH_{ads} corresponds to the enthalpy change for overall adsorption anywhere within the zeolite, including at protons).[40] The Si/Al ratio of the experimental sample was matched to that used in the simulation. This potential was further validated for alkanes adsorbed in CHA (8-MR pores and smaller cages), and ΔH_{ads} determined by CBMC was found to differ from experimental values by only 0.1−0.3 kJ mol^{-1}.[41] Thus, the force field developed is likely to be transferable to zeolites with a wide range of pore sizes; however, a more detailed evaluation of the potential is still needed. Although the previously developed potential has been shown to reproduce overall adsorption properties well in the aforementioned two structures,[13] its accuracy remains unknown for its predictions of specific adsorption properties in zeolites with a wide range of structural features and varying Si/Al ratios. As noted previously and discussed below, we have therefore carried out a comprehensive comparison between CBMC-predicted values of $\Delta H_{ads\text{-}H+}$ and $\Delta S_{ads\text{-}H+}$ and experimental values for alkanes in seven different zeolites.

The Widom test particle insertion method[13,42] was used to probe the energy surface for alkane adsorption in zeolites (i.e., U_{hg}, interaction energies between zeolites and alkanes) at infinite dilution (i.e., the Henry region).[13,43,22,23,44] Several million test particle insertions were carried out to ensure statistically accurate averages. Using the Widom particle method, the enthalpy of adsorption (ΔH_{ads}) can be computed by[23,44]

$$\Delta H_{ads} = \Delta U_{ads} - RT = \langle U_{hg} \rangle - \langle U_h \rangle - \langle U_g \rangle - RT \quad (1)$$

where $\langle U_{hg} \rangle$, $\langle U_h \rangle$, and $\langle U_g \rangle$ are the Boltzmann-weighted averages of the interaction energies of the zeolite-adsorbate, the zeolite, and the gas, respectively. In these calculations, the zeolite framework is treated as rigid and, therefore, the value of U_h is essentially zero. The Henry's law coefficient (K_H) can also be derived from the inserted configurations using the ratio of the average Rosenbluth weights of the adsorbate in the zeolite framework (i.e., $\langle W \rangle$) and in the ideal gas phase (i.e., $\langle W_{ig} \rangle$), respectively;

$$K_H = \frac{1}{\rho_f RT} \frac{\langle W \rangle}{\langle W_{ig} \rangle} \quad (2)$$

where ρ_f is the mass density of the zeolite framework. With eqs 1 and 2, the entropy of adsorption (ΔS_{ads}) can then be calculated from

$$\Delta S_{ads} = \frac{\Delta H_{ads}}{T} + R[1 + \ln(\rho_f RTK_H)] \quad (3)$$

It is important to note that ΔU_{ads}, ΔH_{ads}, ΔS_{ads}, and K_H (denoted as overall adsorption properties) correspond respectively to the adsorption energy, enthalpy, entropy and Henry's coefficient for alkanes located anywhere within the zeolite, which includes adsorbates in a reactant state near Brønsted acidic protons (i.e., specific adsorption) and in siliceous parts of the framework.[13,23]

For alkane cracking, as pointed out in our previous work and in the introduction,[13,43] specific adsorption properties are of particular interest given that they are directly related to the overall catalytic activity for monomolecular cracking. To obtain the properties corresponding to specific adsorption, a domain decomposition approach[13,42] was developed. This method extracts the configurations at reactant states from all inserted trial configurations, allowing one to effectively and directly compute specific adsorption properties at Brønsted acidic protons. The resulting specific adsorption properties for internal energies, enthalpies, the Henry's coefficients, and entropies at protons are denoted as $\Delta U_{ads\text{-}H+}$, $\Delta H_{ads\text{-}H+}$, K_{H-H+}, and $\Delta S_{ads\text{-}H+}$. An inserted alkane configuration is assigned to the reactant state when a C−C bond j is located within a cutoff radius (r_c) of an Al atom positioned at T-site i.[22] A value of j = 1 indicates the terminal bond, while values of 2, 3, etc. indicate nonterminal bonds with larger values corresponding to bonds further away from the terminal bond. Using *n*-hexane as an example, j = 1 (j1) specifies its terminal bond, while j = 3 (j3) refers to its centermost bond and j = 2 (j2) to the bond in between. From the domain decomposition, specific adsorption properties of bond j of an alkane at a particular T-site i, (i.e., $\Delta U_{ads\text{-}H+}(i,j)$ and $K_{H-H+}(i,j)$, the Henry's constant for bond j of a guest alkane adsorbed at T-site i), can be derived from CBMC simulations. By using the aforementioned eqs 1, 2, and 3 with ρ_f becoming $1/V_H{}^+ n_H{}^+$ (where $n_H{}^+$ is the moles of protons per kilogram of zeolite and $V_H{}^+$ is the volume contained within one mole of spheres of cutoff radius, r_c), $\Delta H_{ads\text{-}H+}(i,j)$ and $\Delta S_{ads\text{-}H+}(i,j)$ can then be calculated.[22] To obtain average values of $\Delta H_{ads\text{-}H+}(i,j)$ over all bonds j of an alkane at each T-site i, $\Delta H_{ads\text{-}H+}(i)$ at a T-site i is determined from the Boltzmann-weighted average of $\Delta H_{ads\text{-}H+}(i,j)$ over all C−C bonds j. The value of $\Delta S_{ads\text{-}H+}(i)$ is then determined from the value of $\Delta H_{ads\text{-}H+}(i)$ as described in refs 13 and 22.

Although the aforementioned approach has been shown to predict specific adsorption properties for isolated T-sites in Brønsted-acid zeolites, it lacks the ability to compute specific adsorption properties in zeolites at varying Si/Al ratios (i.e., with multiple Al atoms).[13,22] We have extended the capability of the domain decomposition approach to calculate the specific alkane adsorption in zeolites at varying Si/Al ratios. We utilized Zeo++[45] to construct zeolite structures for a given Si/Al ratio by randomly distributing Al atoms following Lowenstein's rule.[46] For each studied structure at a Si/Al ratio of interest, 10 random samples s were generated. The specific adsorption properties of *n*-alkanes onto all protons in each of the 10 generated samples were sampled directly via the Widom particle insertion method with the domain decomposition approach. The obtained specific internal energy and Henry's coefficients of the bond j of a guest alkane in sample s are represented as $\Delta U_{ads\text{-}H+}(s,j)$ and $K_{H-H+}(s,j)$, respectively. The same notation is used for the specific adsorption enthalpy $\Delta H_{ads\text{-}H+}(s,j)$ and entropy $\Delta S_{ads\text{-}H+}(s,j)$. To obtain averaged adsorption properties of the sample s over j bonds (e.g., $\Delta H_{ads\text{-}H+}(s)$), the same approach as described above was used. Assuming that each of the 10 sampled Al distributions for a given Si/Al ratio is equally probable, the specific adsorption properties for each Si/Al ratio (averaged over the 10 different randomly generated distributions) correspond to the ensemble averages given by

$$\langle \Delta H_{ads-H+} \rangle = \frac{\sum_s f_s \Delta H_{ads-H+}(s) \exp\left(-\frac{\Delta G_{ads-H+}(s)}{RT}\right)}{\sum_s f_s \exp\left(-\frac{\Delta G_{ads-H+}(s)}{RT}\right)} \quad (4)$$

DOI: 10.1021/acs.jpcc.7b11190
J. Phys. Chem. C 2018, 122, 9397−9410

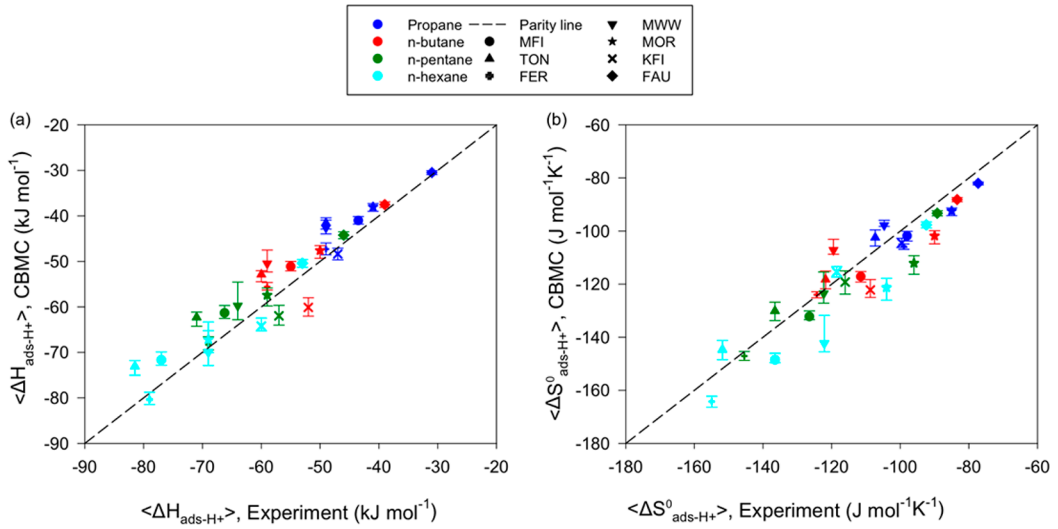

Figure 1. Comparison of specific (a) adsorption enthalpy computed by using a cutoff radius r_c of 5.0 Å (R^2 = 0.85) and (b) standard adsorption entropy ($\Delta S^{\circ}_{ads\text{-}H+}$, corresponding to standard conditions of 1 atm and a fractional coverage 0.5 of acid sites) computed using a cutoff radius r_c of 5.5 Å (R^2 = 0.81) for C3−C6 *n*-alkanes, to experimentally measured values for Brønsted-acidic FAU(2.7), MOR(10), MFI(35), TON(45), FER(30), KFI(4), and MWW(13). The values given in the parentheses indicate the corresponding Si/Al ratio for the material studied. The error bars represent the range of the adsorption properties predicted by CBMC simulations among 10 samples with randomly generated Al distributions (i.e., the highest and lowest value). The R^2 value was calculated using the parity line as the fitted curve.

$$\langle \Delta S_{ads-H+} \rangle = R \ln\left[\sum_s f_s \exp\left(-\frac{\Delta G_{ads-H+}(s)}{RT}\right)\right] + \frac{\langle \Delta H_{ads-H+} \rangle}{T} \quad (5)$$

where f_s is equal to $1/n$ where n is the number of randomly generated Al distributions (in this study, n = 10). We note that, for comparison of the CBMC-calculated values of $\Delta S_{ads\text{-}H+}$ with experimental data, the values of $\Delta S_{ads\text{-}H+}$ determined using eq 5 were further adjusted using eq 20 of ref 22 such that the value of $\Delta S_{ads\text{-}H+}$ has the same reference state as that used in the experimental studies (i.e., pressure of 1 atm and a fractional coverage of acid sites of 0.5, denoted as the standard adsorption entropy, $\Delta S^{\circ}_{ads\text{-}H+}$).

The adsorption selectivity via a central vs a terminal bond is defined as the ratio of the corresponding Henry's coefficients, $K_{H-H+}(j3)/K_{H-H+}(j1)$ or $K_{H-H+}(j2)/K_{H-H+}(j1)$. As an example, the adsorption selectivity at each Si/Al ratio is represented by the ratio of the averaged Henry's coefficient (averaged over 10 samples at each ratio) for central bond adsorption to that for terminal bond adsorption. To better interpret the adsorption selectivity of the central(j3) vs terminal(j1) bonds of *n*-hexane in Brønsted-acid zeolites, density maps were constructed to visualize the configurations of the alkane in j3 and j1 reactant states. For this purpose, CBMC simulations in a canonical (NVT) ensemble were performed with one alkane molecule in the simulation box. More than 30 million Monte Carlo moves including rotation, translation, and reinsertion were carried out, and configurations were collected every 20 attempts. The coordinates of carbon atoms were extracted if they are in the reactant state (within the cutoff radius from the Al atoms). The locations of these coordinates were presented as density maps by projecting onto $x-y$, $x-z$, or $y-z$ planes. The color scale of the maps shows the probability of a C atom being located within square bins of a side length 0.07 Å. Warmer colors on the map (i.e., red vs blue) indicate more thermodynamically favorable configurations.

3. RESULTS AND DISCUSSION

We begin with a discussion of the accuracy and transferability of the adopted force field[13] in describing alkane adsorption in zeolites by comparing the CBMC-predicted specific adsorption properties with available experimental data for seven zeolites having different Si/Al ratios. We then discuss the dependence of the specific adsorption properties on the Si/Al ratios (Al concentrations) and Al spatial distribution, which includes the siting of Al atoms as well as their proximity, to shed light on the observed variation in the central-to-terminal bond selectivity ratio.

3.1. Agreement between Computational Predictions and Experimental Measurements. To facilitate the computational discovery of Brønsted-acid zeolites for alkane cracking, it is of utmost importance to verify the accuracy of simulation predictions. In this study, we carried out a comprehensive comparison between simulations and experimental measurements for the specific adsorption enthalpies and entropies of propane to *n*-hexane in the aforementioned seven zeolites at varying Si/Al ratios. The zeolites studied include FAU(2.7), MOR(10), MFI(35), TON(45), FER(30), KFI(4), and MWW(13) with the Si/Al ratio included in parentheses. The Si/Al ratio is the same for zeolites used in the simulations and in the corresponding experimental studies.[32−35]

As shown in Figure 1a, good agreement is achieved between simulated and experimentally measured values of the specific adsorption enthalpy for C3−C6 *n*-alkanes in zeolites (with an R^2 value of 0.85), clearly suggesting that the force field is accurate and can be transferable to a variety of zeolites with varying Si/Al ratios. It is important to again highlight the fact that the new approach implemented in this study is capable of computing specific adsorption properties in zeolites having different Si/Al ratios. In the previous studies,[43] adsorption properties were computed for isolated T-sites; thus, the simulation results corresponded to relatively high Si/Al ratios. When the Si/Al ratio used in the simulation does not match that of the experimental sample, as shown in the SI, Figure S1, a

DOI: 10.1021/acs.jpcc.7b11190
J. Phys. Chem. C 2018, 122, 9397−9410

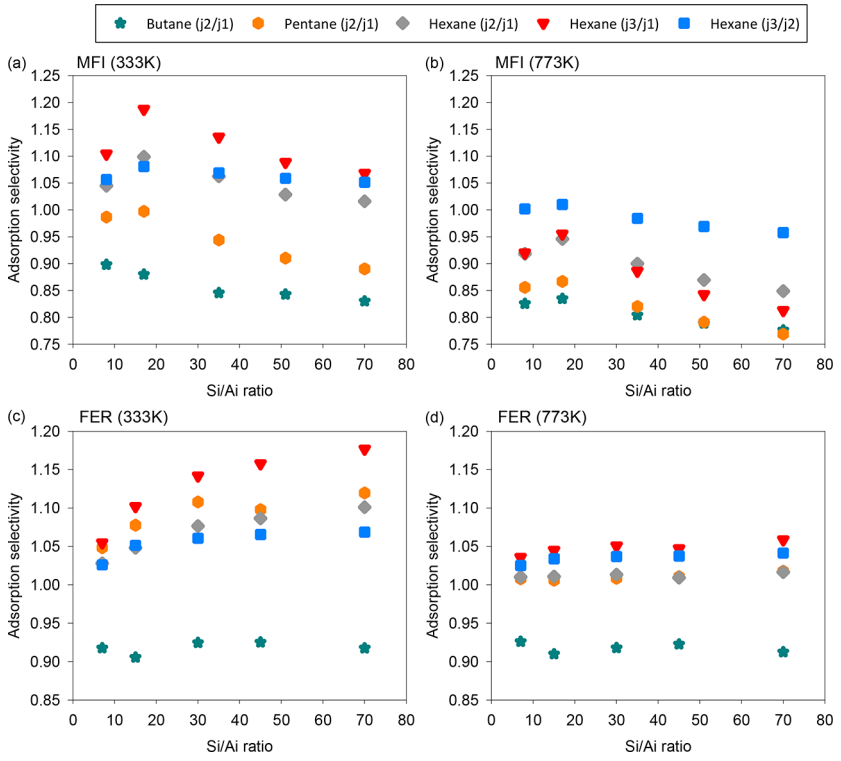

Figure 2. Selectivity ratio for adsorption of a central vs terminal bond for C4−C6 *n*-alkanes adsorbed in Brønsted-acid MFI and FER at Si/Al ratios ranging from 7 to 70 at 333 K and at 773 K (j1 indicates the terminal bond, while j2 and j3 indicate nonterminal bonds with larger values corresponding to bonds closer to the center of the *n*-alkanes).

notable discrepancy between simulations and experiments is found.

Unlike the good agreement achieved for the specific adsorption enthalpies, a systematic discrepancy between the CBMC-determined and experimentally derived specific standard adsorption entropies (see SI Figure S2) was observed. It was found that, as in ref 22, the entropy of adsorption depends critically on the choice of r_c (used to define molecular configurations at the reactant state as discussed in the Computational Method section), whereas the enthalpy of adsorption does not.[22] A value of r_c = 5.5 Å appears to give a reasonable match between the simulations and the entropy of adsorption and the value obtained from experiments, as shown in Figure 1b. However, the agreement of the enthalpy of adsorption with experimental values is relatively insensitive to the cutoff radius for small perturbations of this parameter (see SI Figure S3), as was also found in ref 22. The need for a larger cutoff radius for a better agreement for the entropy might be attributed to how the force field was parametrized. This force field was developed by adjusting only the depth of the potential well (i.e., the ϵ parameter of the 6−12 Lennard-Jones potential), based on parameters for siliceous zeolites, instead of the location of the minimum in the potential (i.e., the σ parameter of the 6−12 Lennard-Jones potential) in order to fit the data to measured overall adsorption enthalpies (i.e., ΔH_{ads}). It is possible that the adsorption distance from the protons calculated using the developed force field has been overestimated to be slightly longer than it should be and therefore, a larger value of r_c is required to compensate for the systematic undercounting of reactant state configurations that results from the lower value (5.0 Å) used previously for r_c. However, considering the uncertainty in the experimental measurements and that the determination of entropies is very sensitive to measured equilibrium adsorption constants, a cutoff radius of 5.0 Å was still used in this study for computing the specific adsorption properties of *n*-alkanes onto protons. This value of the cutoff radius is also consistent with our previous work.[13,43,22,23] In summary, a good agreement between simulations and experiments has been demonstrated for $\Delta H_{ads\text{-}H+}$ and $\Delta S°_{ads\text{-}H+}$. Using the above-described approach, the effects of Si/Al ratios and Al distributions on the specific adsorption of alkanes in Brønsted-acid zeolites are investigated next.

3.2. Effects of Si/Al Ratios on Adsorption Selectivity.

In this section, we systematically investigate the effects of Si/Al ratio on the specific adsorption properties of alkanes at Brønsted-acid sites in different zeolites. As mentioned above, the adsorption selectivity contributes to the reaction selectivity of monomolecular cracking. The adsorption selectivity was calculated as the ratio of the Henry's coefficient for central bonds to that for terminal bonds ($K_{H-H+}(j3)/K_{H-H+}(j1)$ or $K_{H-H+}(j2)/K_{H-H+}(j1)$) averaged over 10 samples with randomly generated Al distributions; see Computational Method for more details). To achieve better central cracking selectivity, one would like to achieve as high a value as possible for this ratio. The value of the central to terminal selectivity ratio was studied for a range of Si/Al ratios from 2 to 71 for C4−C6 *n*-alkanes. In the following discussion, for simplicity and using *n*-hexane as an example, the specific adsorption selectivity of central(j3) vs terminal(j1) bond adsorption is denoted as j3/j1.

Figure 2 shows the central-to-terminal bond selectivity ratio for C4 to C6 *n*-alkanes at 333 and 773 K in two Brønsted-acid zeolites, MFI and FER, as a function of Si/Al ratio. The selectivity presented in the figure is averaged over the 10 randomly generated samples at each ratio. Interestingly, this

DOI: 10.1021/acs.jpcc.7b11190
J. Phys. Chem. C 2018, 122, 9397−9410

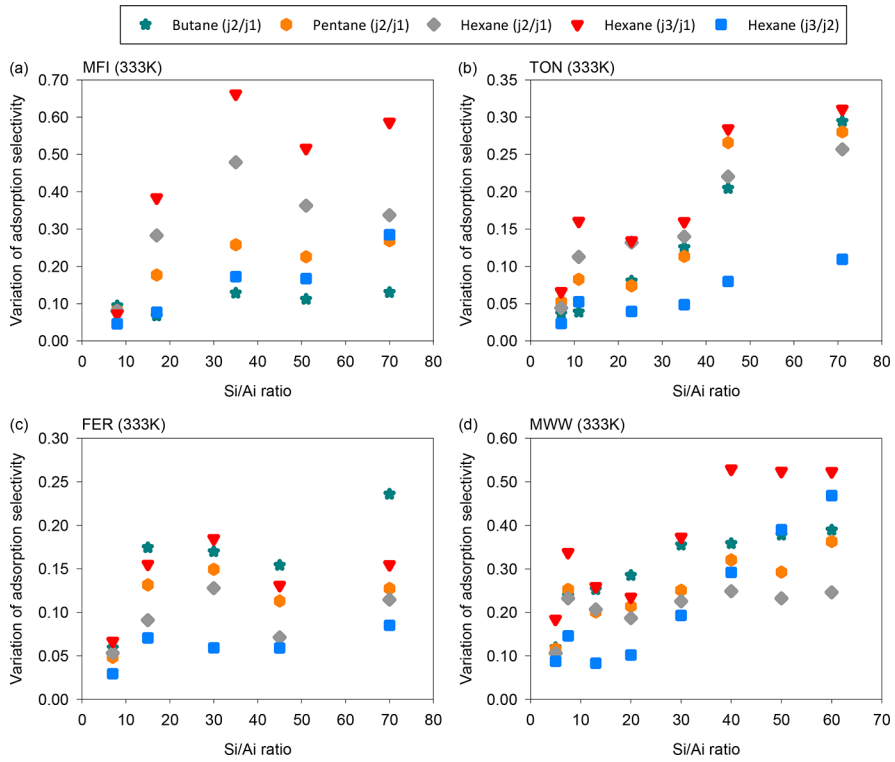

Figure 3. Variation of the adsorption selectivity (defined as the difference between the maximum and minimum value of the selectivity ratio for adsorption of central vs terminal bonds among 10 samples) of C4−C6 *n*-alkanes in Brønsted-acid (a) MFI, (b) TON, (c) FER, and (d) MWW as a function of Si/Al ratio at a temperature of 333 K (j1 indicates the terminal bond while j2 and j3 indicate nonterminal bonds with larger values corresponding to bonds closer to the center of the *n*-alkanes).

figure shows that for some structures, an optimum Si/Al ratio exists that maximizes the central-to-terminal adsorption selectivity. At a Si/Al ratio of 17, MFI shows the highest j3/j1 selectivity of 1.19 for hexane at 333 K, whereas a Si/Al ratio of 70 leads to a lower value of 1.07. The selectivity ratios for *n*-pentane(j2/j1) and *n*-butane(j2/j1) also show an approximately 10% higher selectivity at lower ratios relative to higher ratios. For FER, more favorable selectivity for hexane(j3/j1) was observed at a higher Si/Al ratio, an increasing trend from 1.05 at FER(7) to 1.18 at FER(70). Similar trends hold for hexane(j2/j1), hexane(j3/j2), and pentane(j2/j1) in FER. By contrast, the adsorption selectivity for TON, MWW, MOR, KFI, and FAU (see SI Figures S4 and S5) exhibits essentially no difference in the selectivity ratio as a function of Si/Al ratio. Overall, MFI and FER tend to have a larger j3/j1 selectivity for hexane, although the j3/j2 selectivity is the highest for MFI at 773 K. MWW, MOR, KFI, and FAU have a higher selectivity for hexane(j3/j2), whereas TON shows an opposite trend, namely, that the j3/j2 selectivity for hexane is lowest and the j3/j1 selectivity for butane is the highest. It is interesting that the variations in selectivity as a function of Si/Al ratio are even less pronounced at higher temperature, possibly because the larger thermal motion of the alkane at a high temperature makes the terminal and central bonds become more indistinguishable, resulting in a smaller variation of the selectivity.

In summary, the influence of Si/Al ratio on the selectivity ratio is in general weak and differs qualitatively across framework types. However, it can be inferred that it is the specific interaction of the alkane with multiple protons that drives the observed variation of adsorption properties with Si/Al ratio, since the concentration of proximate or "paired" Al atoms changes with this ratio in zeolites with a random distribution of Al.[47] Rice et al.[47] have shown that the fraction of Al next nearest neighbors varies from 0.64 for a Si/Al ratio of 12 to 0.22 for a Si/Al ratio of 48, if the Al atoms are distributed randomly in MFI. This raises the question of how Al proximity in general affects the adsorption selectivity. The effects of proximate Al atoms cannot be inferred simply by varying the Si/Al ratio, because such an analysis is complicated by the fact that the interaction between proximate protons and adsorbed alkanes is likely to depend in a complex way on the distribution of proximate Al atoms over different T-sites as well as on the total number of Al atoms in close proximity to the alkane. In order to investigate the effects of Al proximity on adsorption in a reactant state systematically and without such complications, the adsorption selectivity was investigated for an Al located at T1 in MFI with a second Al located at different nearby locations, as discussed in section 3.3.3.

3.3. Variation in Adsorption Selectivity. 3.3.1. Effects of Al Distributions. In contrast to the marginal effect of Si/Al ratio, adsorption selectivity was found to vary considerably among different samples (10 samples with randomly generated Al distributions for each zeolite) at a given Si/Al ratio, suggesting that the Al distribution strongly affects the central-to-terminal selectivity. Figure 3 shows the difference between the highest and the lowest selectivity for 10 studied samples at each Si/Al ratio for MFI, TON, FER, and MWW at a temperature of 333 K. Data for FAU, MOR, and KFI are shown in SI Figure S6. In MFI, the selectivity ratio for hexane adsorption (j3/j1) among different Al distributions at a Si/Al ratio of 35 can vary by as much as 0.67 (i.e., largest: 1.46 and lowest: 0.79, a nearly 2-fold difference) at 333 K; such selectivity variation can also be seen in MWW for hexane(j3/

DOI: 10.1021/acs.jpcc.7b11190
J. Phys. Chem. C 2018, 122, 9397−9410

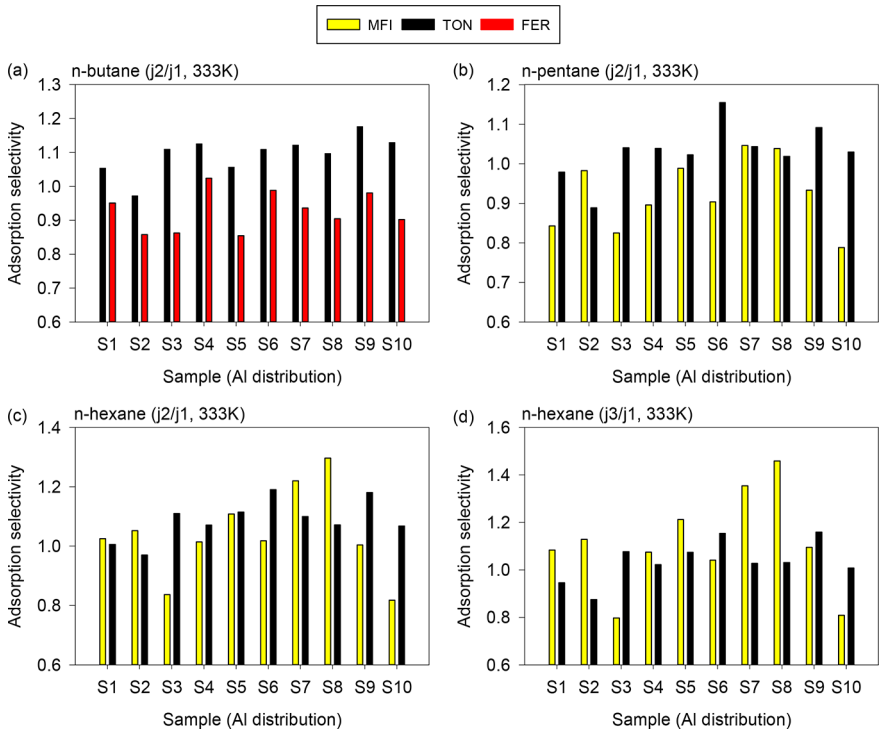

Figure 4. Selectivity ratio for adsorption of a central(j3) vs terminal(j1) bond of C4−C6 *n*-alkanes for 10 samples having different (and randomly generated) Al distributions in Brønsted-acid MFI(35), TON(45), and FER(30) at 333 K. (a) Butane(j2/j1), (b) pentane(j2/j1), (c) hexane(j2/j1), and (d) hexane(j3/j1) (j1 indicates the terminal bond while j2 and j3 indicate nonterminal bonds with larger values corresponding to bonds closer to the center of the *n*-alkanes).

j1) at the Si/Al ratio of 40. As expected, the variation in the selectivity among the 10 samples is again smaller at a higher temperature (i.e., 773 K, see SI Figures S7 and S8) likely due to the larger thermal motion. However, a considerable difference between the maximum and minimum adsorption selectivity—approximately 60% (lowest: 0.71 and highest: 1.10) is still observed (see SI Figure S7). Because the Al distribution differs among the 10 samples, this large selectivity variation suggests that if the Al distributions that lead to high adsorption selectivity could be understood and controlled (discussed below), the specific central-to-terminal adsorption selectivity could be optimized. Moreover, Figures 3 and S6 also show that considerable selectivity variation is observed for Si/Al ratios larger than 10 for most zeolites. This suggests that, for zeolites with a high Si/Al ratio, experimentally measured kinetics or adsorption thermodynamics from a single sample may not be representative of the effects of the zeolite structure in aggregate.

In general, our results show that the selectivity of hexane(j3/j1) adsorption exhibits the largest variation at a given Si/Al ratio, which indicates that the adsorption selectivity ratio for larger alkanes is more sensitive to the Al distribution. In other words, the adsorption affinities of the central and terminal bonds of larger alkanes show a higher sensitivity to the Al distribution. We therefore anticipate that the variation in central-to-terminal selectivity would probably become even larger for longer alkane molecules. It is therefore interesting that the variation in selectivity is larger for butane relative to hexane in FER, which may be a consequence of a better match between the size of the FER cage and the size of a butane molecule. Therefore, butane may be able to adopt some specific configurations within FER at certain Al distributions, resulting in a larger variation of the adsorption selectivity.

To investigate the effect of the Al distribution on adsorption selectivity in greater detail, we next examine the selectivity ratios for each of the 10 samples generated for a given Si/Al ratio. We focus our attention on zeolites with Si/Al ratios identical to those used previously for the comparison of adsorption thermodynamic data between simulations and experiments (i.e., MFI(35), FAU(2.7), MOR(10), TON(45), FER(30), KFI(4), and MWW(13)). The selectivity of butane-(j2/j1) for each sample of FER and TON, and of pentane and hexane for each sample of TON and FER (10 samples per zeolite) is shown in Figure 4. Data for alkanes adsorbed in the remaining zeolites are presented in the SI, Figures S9 and S10. Large differences in selectivity among samples can clearly be seen, in particular for hexane(j3/j1) in MFI(35). As shown in Figure 4d, sample #3 (denoted as S3) of MFI(35) exhibits a selectivity of 0.79, while S8 exhibits a value of 1.46; also, S2 of TON(45) exhibits a selectivity of 0.87, while S9 exhibits a value of 1.16. The data for *n*-hexane(j2/j1) are presented in Figure 4c, and similar differences in the selectivity are observed between S10 and S8 for MFI(35). The selectivity for butane(j2/j1) differs by as much as 0.2 among different Al distributions in FER(30) and TON(45), as shown in Figure 4(a). Likewise, notable variation for pentane(j2/j1) among different samples can be seen in Figure 4b. By contrast, FAU(2.7) and KFI(4) exhibit little variation as shown in SI Figures S9 and S10, which can be attributed to their low Si/Al ratios. To shed light on the observed variation of adsorption selectivity among different Al distributions for a given zeolite framework, two factors are identified below that influence this variation: (1) the siting of Al atoms at specific T-sites and (2) the spatial proximity of Al atoms.

3.3.2. Effects of Al Siting at Specific T-Sites. We begin by investigating the adsorption selectivity at each of the 12

DOI: 10.1021/acs.jpcc.7b11190
J. Phys. Chem. C 2018, 122, 9397−9410

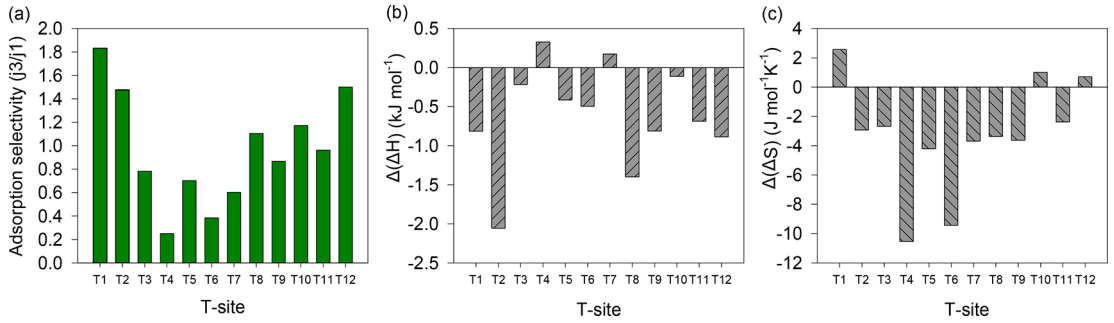

Figure 5. (a) Selectivity ratio for adsorption of central(j3) vs terminal(j1) bonds of *n*-hexane at each of the 12 distinct T-sites of Brønsted-acid MFI, (b) the difference in the adsorption enthalpy between j3 and j1, and (c) the difference in the adsorption entropy between j3 and j1. The average uncertainties for values for $\Delta(\Delta H)$ and $\Delta(\Delta S)$ are 0.46 kJ mol^{-1} and 1.09 J mol^{-1} K^{-1}, respectively. These values were determined by comparing results obtained using half the number of Monte Carlo cycles relative to that used to obtain the data reported in this figure.

distinct T-sites of MFI. The calculations used to obtain the adsorption properties at each T-site were performed for structures having only one active site and, therefore, a high Si/Al ratio. Figure 5a shows the adsorption selectivity for each T-site of MFI. It can be seen that there is a wide range of the selectivity ratio j3/j1 for hexane among the different sites. T1 is the most selective T-site with a selectivity ratio of 1.83, whereas T4 exhibits the lowest selectivity ratio of 0.25, a difference of a factor of ∼7 relative to the value for T1. The variation in the observed j3/j1 adsorption selectivity ratio can be attributed to differences in the specific enthalpy ($\Delta H_{ads\text{-}H+}$) and entropy ($\Delta S_{ads\text{-}H+}$) of adsorption between j3 and j1 bonds at a given T-site (defined respectively as $\Delta(\Delta H)$ and $\Delta(\Delta S)$), since the ratio of the Henry's coefficients for the two bonds is proportional to the difference in $\Delta G_{ads\text{-}H+}$.[14] Values of $\Delta H_{ads\text{-}H+}$ and $\Delta S_{ads\text{-}H+}$ for j3 and j1 adsorption at each T-site can be found in the SI, Tables S1 and S2. The values of $\Delta(\Delta H)$ and $\Delta(\Delta S)$ are shown respectively in Figure 5b,c. It can be seen that the high selectivity ratio observed for T1 is driven by both energetically stronger j3 adsorption (i.e., negative $\Delta(\Delta H)$ relative to j1 adsorption) as well as by lower confinement of the alkane (positive $\Delta(\Delta S)$) for j3 relative to j1 adsorption. Similar effects of $\Delta(\Delta H)$ and $\Delta(\Delta S)$ on the selectivity can be seen for T12, which also exhibits high selectivity for j3 adsorption. On the other hand, the poor selectivity observed for T4 is due to a large entropy penalty for j3 vs j1 adsorption (i.e., negative $\Delta(\Delta S)$). This T-site is located in the sinusoidal channels of MFI; and the negative value for $\Delta(\Delta S)$ suggests that the molecule is more confined when adsorbed in a j3 reactant state vs a j1 reactant state at these locations. At T2 and T8 sites, the enthalpy stabilization for j3 (i.e., negative $\Delta(\Delta H)$) is the dominating factor contributing to the relatively high selectivity. These sites can be described as located in the intersection and straight channels. The competition between $\Delta(\Delta H)$ and $\Delta(\Delta S)$ in determining the observed differences in selectivity among T-sites is expected to be controlled primarily by the local geometry of the T-site, as discussed below.

We have found that a large variation of the selectivity ratio among the 10 samples of a given Si/Al ratio (having randomly generated Al distributions as described in section 3.2) is related to the range of the adsorption selectivity observed among individual T-sites of the zeolite as described above. As shown in Figure 6, a clear relationship exists between the selectivity variation among the 10 different samples and the range of adsorption selectivities among distinct T-sites of the zeolites studied. It is noted that Si/Al ratios of 16 and 50 were used for FAU and KFI, respectively, in Figure 6 instead of the values of

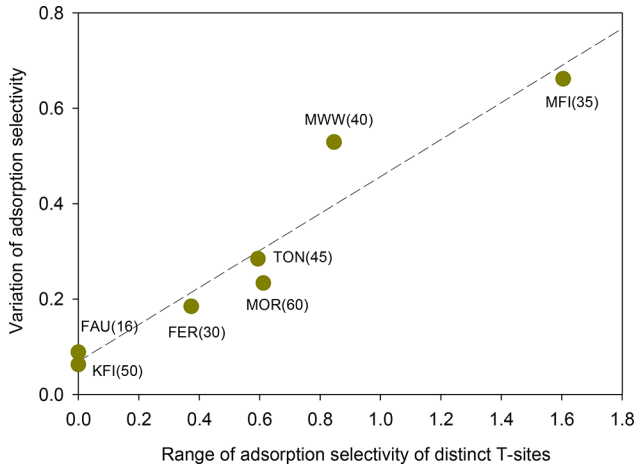

Figure 6. Difference between the highest and lowest values of the adsorption selectivity ratio for central(j3) vs terminal(j1) bonds of *n*-hexane among 10 different samples of a given Si/Al ratio at 333 K (the 10 samples of each zeolite structure have random distributions of Al as described in section 3.2), vs the range in the selectivity ratio among distinct T-sites of Brønsted-acid zeolites, labeled on the figure, with Si/Al ratios larger than 10. (Si/Al ratios are given in parentheses.)

2.7 and 4 used in section 3.1. The larger Si/Al ratios were chosen for the preset analysis because, as discussed in section 3.3, higher Si/Al ratios exhibit greater variability in the selectivity ratio among samples; thus, to allow for direct comparison of data points in Figure 6, large (i.e., > 10) Si/Al ratios were employed. The vertical axis corresponds to the difference between the maximum and minimum value of the adsorption selectivity ratio across the 10 samples having different Al distributions, while the horizontal axis gives the difference between the maximum and minimum selectivity ratio among distinct T-sites (inaccessible T-sites possessing a Gibbs free energy of adsorption larger than 5 kJ/mol at 333 K were excluded).

These results can be used to explain why MFI exhibits the largest variation in selectivity among 10 samples of a given Si/Al ratio, followed by MWW (as seen in Figure 3). For large Si/Al ratios the range in selectivity ratio among different samples with randomly generated Al distributions is expected to converge to the range of selectivity ratios among the individual isolated T-sites; Figure 6 shows that the range for individual T-sites is largest for MFI and MWW. This observation also suggests that the variation in selectivity among individual T-sites can serve as a good descriptor for identifying zeolites

DOI: 10.1021/acs.jpcc.7b11190
J. Phys. Chem. C 2018, 122, 9397−9410

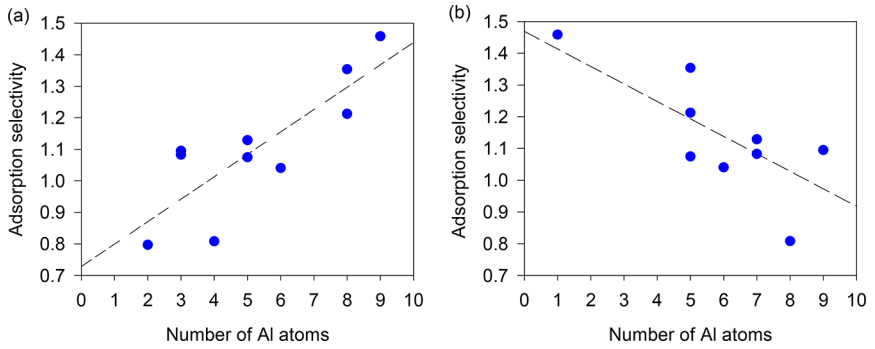

Figure 7. Selectivity ratio for adsorption of a central(j3) vs terminal(j1) bond of *n*-hexane in Brønsted-acid MFI vs the number of Al atoms located at the (a) three most selective T-sites (T1, T2, T12) and (b) four least selective T-sites (T4, T5, T6, and T7) for the studied Brønsted-acid MFI(35) samples (i.e., 10 samples having random Al distributions and a Si/Al ratio of 35).

whose adsorption properties (and, by extension, cracking selectivities) may be very sensitive to the siting of Al atoms. For such structures, the adsorption thermodynamics and cracking kinetics for a given sample may not be representative of the zeolite structure in aggregate. Thus, it is important to average over different samples when comparing rate or adsorption data across different zeolites having such structures.[13] On the other hand, for zeolites that are identified to have large variation in the adsorption properties among T-sites, the cracking selectivity could potentially be tuned by controlling the Al distribution. The ability to do so would also be desirable when structural heterogeneity is desired, for example, to permit only certain reactants to enter the zeolite via channels, but where it is desired that the reaction take place at cages or other locations with significantly different adsorption properties.

The high adsorption selectivity observed for some of the 10 samples studied for MFI(35) at 333 K was found to correlate strongly with the number of Al atoms sited at individual T-sites in the structure having high selectivity. Figure 7a shows a plot of the adsorption selectivity ratio for MFI vs the number of Al atoms located in sites T1, T2, and T12. The same correlation is observed if only the number Al atoms at T1 (which has the highest selectivity) is counted (see SI Figure S11). Conversely, a negative correlation is observed between the selectivity ratio and the number of Al atoms at sites T4, T5, T6, and T7 (the four least selective sites) in the structures, as shown in Figure 7b. The same relationship was also found for *n*-hexane in MFI(35) at 773 K. Even at this elevated temperature, sample S8 still exhibits the highest j3/j1 selectivity ratio, and site T1 is still the most selective T-site (see SI Figure S12). However, it should be noted that, depending on the relative importance of entropic vs enthalpic effects at different temperatures, the most selective of the 10 samples and the most selective T-sites may change. The correlations seen in Figure 7 demonstrate again the important role of Al siting in determining the adsorption selectivity. A zeolite with more Al atoms sited at more selective T-sites will exhibit a higher overall adsorption selectivity and vice versa. Accordingly, a broader spectrum of adsorption selectivity ratios among different T-sites in a zeolite is anticipated to lead to a larger variation in selectivity ratios among different Al distributions.

These results demonstrate that the siting of Al atoms at T-sites exhibiting high or low j3/j1 selectivity strongly determines the adsorption selectivity, and indicate that a desirable Al distribution should contain Al atoms sited at those locations possessing high adsorption selectivity for central bond adsorption. Therefore, it is important that a computational screening study with the aim of identifying promising zeolite candidates for future experimental investigations should include calculations for each T-site of a zeolite. It is noted that previous experimental studies have demonstrated the possibility of synthesizing zeolites with Al atoms located at particular T-sites.[48−50] Han et al.[51] have shown evidence for nonrandom siting of Al in MFI using Al MAS and MQ MAS NMR. Sklenak et al.[52] have concluded that the siting of Al atoms in framework T-sites depends on the conditions of zeolite synthesis. These experimental studies and several other studies[53−56] support the possibility of targeting preferred Al siting via advanced synthesis methods, thus providing opportunities to enhance the cracking selectivity at central vs terminal C−C bonds. We note also that the relationship established in the present study may also be used to reverse engineer the Al siting of Brønsted-acid zeolites. The differences in the experimentally measured adsorption properties between samples synthesized under different conditions can be compared to our computational results to inform the possible siting of Al atoms within the experimental samples. For instance, using MFI as an example, if a given sample shows a substantially higher selectivity ratio than others, this indicates that the sample might have a larger fraction of Al atoms located at T1 and/or T12, T-sites identified to possess a large selectivity ratio.

To unravel the effects of the local environment surrounding a T-site on the adsorption selectivity, we have also investigated the local geometry of the most selective T-site for hexane(j3/j1) adsorption at 333 K in each of the seven zeolites studied. The selectivity ratios for these T-sites range from 0.4 (for KFI site T1) to 1.83 (for MFI site T1). The structural files for the local geometry of these seven T-sites can be found in the Supporting Information. Overall, it was found that a more confined space generally leads to a higher selectivity ratio for adsorption via central C−C bonds relative to terminal ones. For instance, T1(FAU) and T1(KFI), both located in large cages approximately 15 Å in diameter (without excluding the van der Waals radii of the framework atoms), have a selectivity ratio that is 2 times lower than that of T4(MOR), located at a channel with a size of nearly 10 Å. T-sites such as T1(FER) are situated within a channel of about 7 Å in diameter and exhibit a higher selectivity ratio (1.35) compared to that of T4(MOR) (1.17). These simple descriptors (e.g., pore or cage size), however, are inadequate for fully describing the local geometry and, therefore, its effects on the selectivity ratio.[14] For example, T1(MFI), which is also located in a channel ∼7 Å in diameter, has a selectivity ratio of 1.83, higher than that for T1(FER). Its location near the intersection of the straight and sinusoidal

DOI: 10.1021/acs.jpcc.7b11190
J. Phys. Chem. C 2018, 122, 9397−9410

channels may be slightly less confining toward j3 adsorption relative to T1(FER), resulting in higher selectivity of central vs terminal C−C bond adsorption, but this subtle difference in local environment is not easily captured by one characteristic dimension. Additionally, T5(MWW) is located in a side pocket, which is anticipated to exhibit adsorption properties that are also not captured easily by a single channel or cage diameter. More realistic geometry descriptors (e.g., length of channel/cage segments, surface curvature) are therefore needed to describe the local geometry at T-sites in order to achieve quantitatively improved understandings of the effects of structure on adsorption. Such a study is outside the scope of the present work, and will be an important subject of a future investigation.

3.3.3. Effects of Al Spatial Proximity. In addition to the Al distribution among T-sites, the spatial proximity of individual Al atoms was found to influence the adsorption selectivity of alkanes in zeolites, as discussed in this section. To facilitate the discussion, *n*-hexane and MFI(35) are again used as examples and the adsorption configurations of the j3 and j1 bonds are visualized for two of the 10 samples using density maps, presented in SI Figure S13. Maps are presented for samples 3 and 8, which exhibited the lowest and highest selectivity to j3 adsorption, respectively, among the 10 total samples. It can be seen that j3 adsorption is more thermodynamically favored in sample 8, based on the warmer colors (e.g., red vs blue) seen on the density map for sample 8 vs sample 3. It can also be seen that the j3 configurations are highly concentrated within the circled region of the figure, and that Al atoms are in close proximity in this region. A ball and stick model of part of the zeolite structure within the region is shown in SI Figure S14, which shows that four Al atoms are located in close proximity within four adjacent rings. This observation suggests that proximate Al sites may play a role in the adsorption selectivity. To understand such an effect, simplified systems having a variety of Al pairs centered on T1 (the most selective T-site) were studied. Specifically, 12 systems were investigated containing 12 different pairs (i.e., T1−T1, T1−T2, ..., and T1−T12 pairs located in different rings of MFI). The locations of the T-sites within the framework structure are identified in the ball and stick model shown in Figure 8.

Figure 9 shows the j3/j1 adsorption selectivity for hexane in MFI for each Al pair. As a comparison, we have also computed

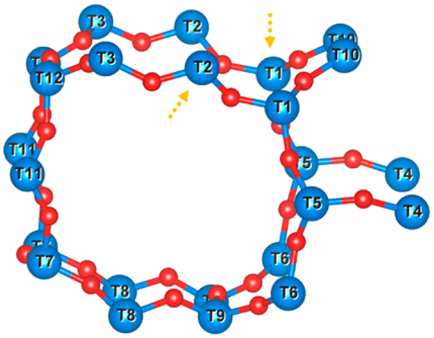

Figure 8. Relative position of different T-sites shown in a cluster structure of MFI. The two arrows indicate a pair consisting of Al at T1 and at T2 located in close proximity, with the T-sites located in different rings. It is noted that all Al pairs studied in this work are located within different rings (Color code - O atoms: red; Si atoms: blue).

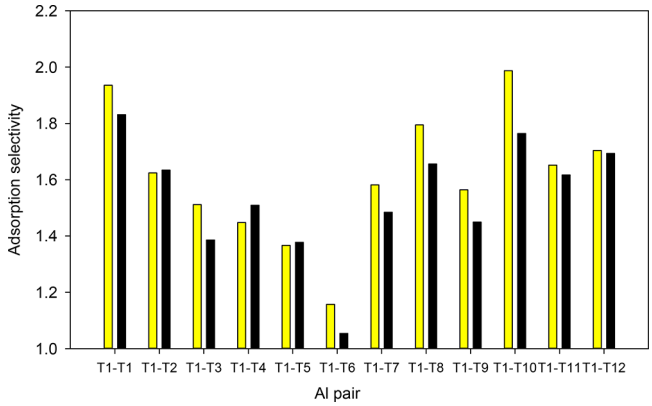

Figure 9. Selectivity ratio for adsorption of a central(j3) vs terminal(j1) bond of *n*-hexane in Brønsted-acid MFI possessing different pairs of Al atoms located in close proximity to one another. The yellow bars (left) indicate two Al atoms located in close proximity. The black bars (right) indicate two Al atoms located far apart.

the adsorption selectivity for the case where the members of Al pairs are located far away from each other. The results show that the pairing of Al sites can indeed enhance the selectivity to j3 adsorption. For example, by comparing the selectivity of a T1−T10 pair in close proximity to that of a well-separated pair, it can be seen that the presence of a T10 Al site near a T1 site raises the selectivity by 12.7%. Similar results are observed for other pairs such as T1−T1, T1−T8, and T1−T9. Interestingly, we found that the close proximity of Al atoms can also reduce the selectivity to j3 adsorption. For example, the structure with a T1−T4 pair in close proximity exhibits a lower selectivity compared to that of a well separated T1−T4 pair. Notably, experimental studies have also shown that the population of Al pairs can be tuned in MFI, and possibly also in other Si-rich zeolites.[57−61] These results indicate that the placement of Al sites in close proximity to one another may be another key design parameter that can be used to manipulate the adsorption selectivity for alkane adsorption and cracking.

We propose that the observed effect of Al proximity on adsorption selectivity relative to isolated Al sites originates from a complex trade-off between energetic and entropic factors introduced by a neighboring Al site. To understand the origins of the effects of neighboring Al atoms on adsorption, density maps are presented in Figure 10 of the configurations of j1 and j3 bonds of hexane adsorbed near paired T1−T10 sites and near individual T1 and T10 sites (data are projected onto the $x-y$ plane; density maps projected onto the $x-z$ and $y-z$ planes can be found in the SI, Figures S15 and S16, respectively). By comparing these density maps, it can be seen that the adsorption of a central bond (j3) for hexane is notably enhanced when T1 and T10 are in close proximity (see Figure 10d) relative to the individual T1 and T10 sites (see Figure 10e,f, respectively). Thus, Al atoms in proximate T1 and T10 sites stabilize the adsorption of hexane via the j3 bond, relative to adsorption at protons associated with isolated Al atoms at the T1 or T10 sites. It is noted that the adsorption of the j1 bond near the paired sites (see Figure 10a) is also enhanced, compared to the individual T1 and T10 sites (see Figure 10b,c, respectively), but the enhancement is weaker, resulting in a higher j3/j1 selectivity ratio for the paired sites. Thus, with some arrangements of neighboring T-sites, the second Al site provides an additional interaction relative to an

DOI: 10.1021/acs.jpcc.7b11190
J. Phys. Chem. C 2018, 122, 9397−9410

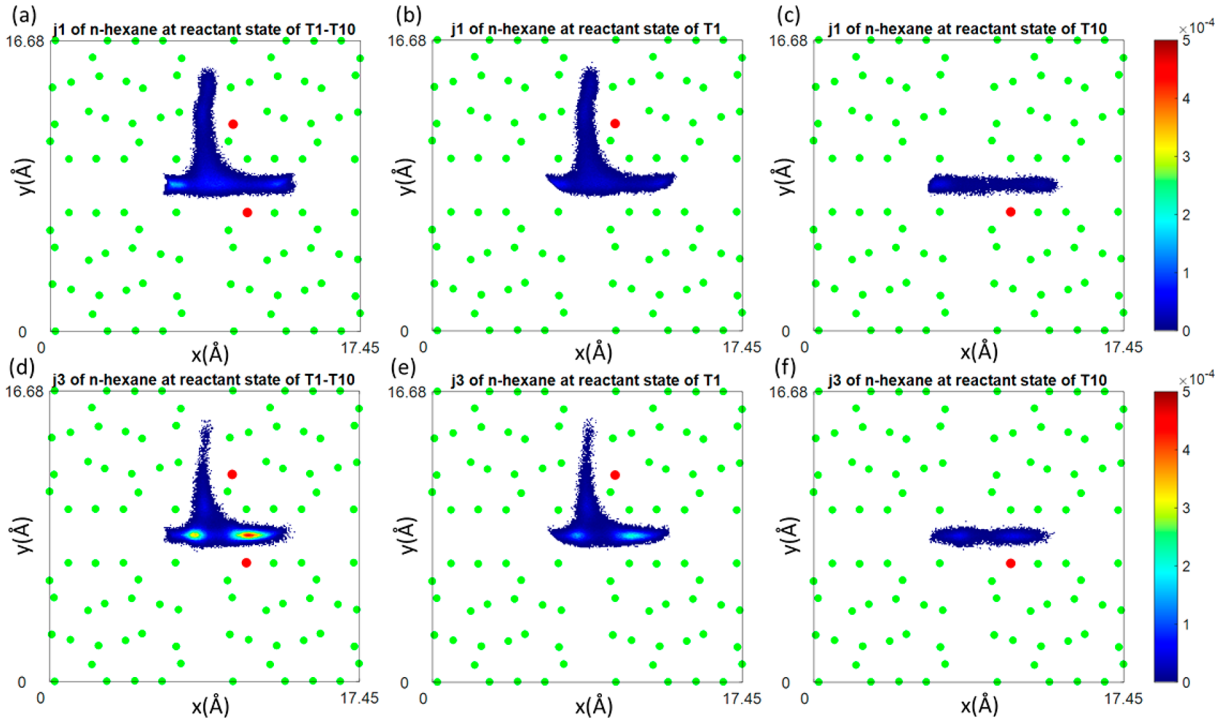

Figure 10. Density maps, projected onto the $x-y$ plane, of the (a–c) terminal(j1) and (d–f) central(j3) bond configurations of *n*-hexane adsorbed in Brønsted-acid MFI at (a,d) a T1-T10 pair with Al atoms located in close proximity, and at isolated (b,e) T1, and (c,f) T10 sites (Color code - green dots: Si atoms; red dots: Al atoms). The color bar reflects the probability of either the j1 or j3 bond being located within square bins of a side length 0.07 Å, with warmer colors representing more favorable positions for adsorption.

isolated site such that adsorption of the central bond of the alkane is more preferred relative to the terminal bond, enhancing the selectivity.

The above results can be used to interpret the effect of Si/Al ratio on the adsorption selectivity, discussed in section 3.2. Based on the results presented above, the observed maximum in the selectivity ratio for MFI as a function of Si/Al ratio can be partly explained by the enhancement of the selectivity to central(j3) adsorption associated with Al atoms in close proximity. Using the hexane(j3/j1) selectivity ratio as an example, it can be seen (Figure 2) that the selectivity ratio generally increases as the Si/Al ratio decreases. Given that the probability of finding proximate Al atoms increases as the Si/Al ratio decreases, the larger concentration of Al atoms in close proximity at lower Si/Al ratios may promote the adsorption of central vs terminal bonds. However, after reaching a maximum near a Si/Al ratio of approximately 15, the (j3/j1) selectivity ratio decreases as the Si/Al ratio decreases further. For Si/Al ratios less than 10, it is likely that the Al atom concentration is sufficiently high that the fraction of Al in more complicated ensembles involving, for example, three or more Brønsted-acid sites in proximity may increase. Further study is needed in order to understand these multibody effects on the selectivity ratio. In addition, in contrast to MFI, the selectivity ratio for *n*-alkanes in some other structures (e.g., FER) was found to decrease as the Si/Al ratio decreases, the opposite of what is observed for MFI. This result indicates that in some cases, the effects of Al atoms being present as pair is to reduce, rather than increase, the selectivity for central C–C adsorption. The effects of the Al proximity on adsorption selectivity is thus expected to be a complex function of characteristics such as the zeolite structure and the siting of the Al pairs.

4. CONCLUSIONS

In this work, we investigated the effects of Si/Al ratio and Al distribution on the central-to-terminal bond adsorption selectivity of *n*-alkanes in Brønsted-acid zeolites. A new computational approach was implemented, which allows us to calculate the specific adsorption of *n*-alkanes in Brønsted-acid zeolites at different Si/Al ratios. We first verified that the force field used for this work is accurate and transferable, by comparing the simulation results with experimental data for seven zeolites having a range of Si/Al ratios. While optimal Si/Al ratios, for which the selectivity of central vs terminal bond adsorption is maximized, were found to exist for MFI and FER, we also found that the correlation of adsorption selectivity with the Si/Al ratio is relatively weak and does not play a crucial role in determining the selectivity; the selectivity to adsorption of *n*-hexane via a central(j3) vs terminal(j1) bond remains approximately constant as a function of Si/Al ratio. The Al distribution, on the other hand, was found to significantly affect the adsorption selectivity, and this effect becomes more pronounced when the Si/Al ratio is larger. A nearly two-fold difference in the j3/j1 adsorption selectivity ratio for hexane at 333 K was observed among 10 samples of MFI having random distributions of Al and a Si/Al ratio of 35. Although such variation in the selectivity with respect to the Al distribution becomes smaller at 773 K, a difference in the j3/j1 ratio of as high as 60% can still be observed among the 10 samples.

Two main factors—the siting of Al at different T-sites, as well as the spatial proximity of Al atoms—were found to contribute significantly to the observed variation in adsorption selectivity among 10 samples of a given zeolite structure having different Al distributions. The variation in selectivity among the 10 samples strongly correlated with the variation of the selectivity among individual isolated T-sites. For example, a

DOI: 10.1021/acs.jpcc.7b11190
J. Phys. Chem. C 2018, 122, 9397–9410

higher ratio of the selectivity for central vs terminal bond adsorption of *n*-hexane(j3/j1) in MFI having a Si/Al ratio of 35 corresponded to Al distributions in which a high fraction of Al is located at T-sites exhibiting high selectivities as isolated sites. Our study shows that T-sites located in a more confined space tend to possess a higher selectivity to central bond adsorption, indicating that the ability to tune the Al distribution among T-sites having different local environments would allow for control of the adsorption selectivity. However, further study is needed in order to establish a quantitative relationship between local geometry and adsorption selectivity. Proximate Al atoms were also found to influence the j3/j1 adsorption selectivity ratio for hexane, albeit less strongly than the distribution of Al among T-sites. Density maps of the configurations of the bonds of *n*-hexane adsorbed within MFI having a Si/Al ratio of 35 show that adsorption of the j3 C−C bond can be more favored relative to adsorption of the j1 C−C bond when two Al atoms are present in proximate T sites. Therefore, tuning the Al proximity may offer an additional design parameter to improve the selectivity ratio.

Overall, our results clearly demonstrate that the central-to-terminal selectivity ratio for C−C bond adsorption in zeolites depends primarily on the distribution of Al atoms among the framework T sites, in particular for zeolites having a high Si/Al ratio. As discussed above, recent studies have shown that through the use of advanced zeolite synthesis methods, Al atoms in some zeolites can be placed strategically at specific T-sites, and the distribution of Al atom pairs can also be tailored using known synthesis techniques. The ability to control the Al siting in zeolites such as MFI and other frameworks possessing heterogeneous pore systems, and thus a large range of the selectivity ratio among different T-sites, would provide opportunities to significantly enhance the selectivity to adsorption of a given C−C bond of an alkane. Given that our recent work has shown that zeolites that are more confining and, therefore, more selective to central C−C bond adsorption, are also more intrinsically selective to cracking of central vs terminal C−C bonds, the ability to computationally screen zeolites based on adsorption selectivity also provides a means for identifying zeolites and/or T-sites that will promote cracking at central locations of an alkane. We anticipate that the findings of this study can be used to guide the rational placement of Brønsted-acid sites.

■ ASSOCIATED CONTENT

Supporting Information

The Supporting Information is available free of charge on the ACS Publications website at DOI: 10.1021/acs.jpcc.7b11190.

Additional figures comparing simulations and experiments (section 3.1) when inconsistent Si/Al ratios or different cutoff radii are used; additional figures showing the effects of Si/Al ratios (section 3.2) and Al spatial distributions (section 3.3, including effects of Al proximity) on the specific adsorption selectivity of *n*-alkanes in varying Brønsted-acid zeolites studied in this work at 333 and 773 K; tables for the specific adsorption enthalpy and entropy of the central and terminal bonds of hexane at each of the 12 distinct T-sites in Brønsted-acid MFI (PDF)

■ AUTHOR INFORMATION

Corresponding Authors

*E-mail: bell@cchem.berkeley.edu.
*E-mail: lin.2645@osu.edu.

ORCID

Amber Janda: 0000-0001-8545-448X
Alexis T. Bell: 0000-0002-5738-4645
Li-Chiang Lin: 0000-0002-2821-9501

Present Address

§Department of Chemical Engineering, Stanford University, Stanford, CA 94305, USA

Author Contributions

The study was developed and completed through contributions by all authors.

Notes

The authors declare no competing financial interest.

■ ACKNOWLEDGMENTS

The authors gratefully thank the Ohio Supercomputer Center (OSC) for providing computational resources to carry out this work.[62] A.T.B. and A.J. acknowledge support from Chevron Energy Technology Company.

■ REFERENCES

(1) Yilmaz, B.; Müller, U. Catalytic Applications of Zeolites in Chemical Industry. *Top. Catal.* **2009**, *52*, 888−895.
(2) Kusakabe, K.; Kuroda, T.; Murata, A.; Morooka, S. Formation of a Y-Type Zeolite Membrane on a Porous α-Alumina Tube for Gas Separation. *Ind. Eng. Chem. Res.* **1997**, *36*, 649−655.
(3) Sherry, H. S.; Walton, H. F. The Ion-Exchange Properties of Zeolites. II. Ion Exchange in the Synthetic Zeolite Linde 4A. *J. Phys. Chem.* **1967**, *71*, 1457−1465.
(4) Degnan, T. F., Jr. Applications of Zeolites in Petroleum Refining. *Top. Catal.* **2000**, *13*, 349−356.
(5) Vermeiren, W.; Gilson, J.-P. Impact of Zeolites on the Petroleum and Petrochemical Industry. *Top. Catal.* **2009**, *52*, 1131−1161.
(6) Kesraoui-Ouki, S.; Cheeseman, C. R.; Perry, R. Natural Zeolite Utilisation in Pollution Control: A Review of Applications to Metals' Effluents. *J. Chem. Technol. Biotechnol.* **1994**, *59*, 121−126.
(7) O'Connor, P. Catalytic Cracking: The Future of an Evolving Process. *Stud. Surf. Sci. Catal.* **2007**, *166*, 227−251.
(8) Jentoft, F. C.; Gates, B. C. Solid-Acid-Catalyzed Alkane Cracking Mechanisms: Evidence from Reactions of Small Probe Molecules. *Top. Catal.* **1997**, *4*, 1−13.
(9) Kotrel, S.; Knözinger, H.; Gates, B. C. The Haag-Dessau Mechanism of Protolytic Cracking of Alkanes. *Microporous Mesoporous Mater.* **2000**, *35*−*36*, 11−20.
(10) Haag, W. O.; Dessau, R. M. Duality of Mechanism of Acid-Catalyzed Paraffin Cracking. In *Proceedings of The Eighth International Congress On Catalysis*; Verlag Chemie: Weinheim, Germany, 1984; p 305.
(11) Kissin, Y. V. Chemical Mechanisms of Catalytic Cracking over Solid Acidic Catalysts: Alkanes and Alkenes. *Catal. Rev.: Sci. Eng.* **2001**, *43*, 85−146.
(12) Caeiro, G.; Carvalho, R. H.; Wang, X.; Lemos, M. A. N. D. A.; Lemos, F.; Guisnet, M.; Ramôa Ribeiro, F. Activation of C2−C4 Alkanes over Acid and Bifunctional Zeolite Catalysts. *J. Mol. Catal. A: Chem.* **2006**, *255*, 131−158.
(13) Janda, A.; Vlaisavljevich, B.; Lin, L.-C.; Smit, B.; Bell, A. T. Effects of Zeolite Structural Confinement on Adsorption Thermodynamics and Reaction Kinetics for Monomolecular Cracking and Dehydrogenation of N-Butane. *J. Am. Chem. Soc.* **2016**, *138*, 4739−4756.
(14) Janda, A.; Vlaisavljevich, B.; Smit, B.; Lin, L.-C.; Bell, A. T. Effects of Pore and Cage Topology on the Thermodynamics of N

DOI: 10.1021/acs.jpcc.7b11190
J. Phys. Chem. C 2018, 122, 9397−9410

-Alkane Adsorption at Brønsted Protons in Zeolites at High Temperature. *J. Phys. Chem. C* **2017**, *121*, 1618−1638.
(15) Kulprathipanja, S.; James, R. B. Overview in Zeolites Adsorptive Separation. In *Zeolites in Industrial Separation and Catalysis*; Wiley-VCH Verlag GmbH & Co. KGaA: Weinheim, Germany, 2010; pp 173−202.
(16) Sohn, S. W. Liquid Industrial Non-Aromatics Adsorptive Separations. In *Zeolites in Industrial Separation and Catalysis*; Wiley-VCH Verlag GmbH & Co. KGaA: Weinheim, Germany, 2010; pp 249−272.
(17) Calero Diaz, S. Modeling of Transport and Accessibility in Zeolites. In *Zeolites and Catalysis*; Wiley-VCH Verlag GmbH & Co. KGaA: Weinheim, Germany, 2010; pp 335−360.
(18) Schenk, M.; Smit, B.; Vlugt, T. J. H.; Maesen, T. L. M. Shape Selectivity in Hydrocarbon Conversion. *Angew. Chem., Int. Ed.* **2001**, *40*, 736−739.
(19) Schenk, M.; Calero, S.; Maesen, T. L. M.; van Benthem, L. L.; Verbeek, M. G.; Smit, B. Understanding Zeolite Catalysis: Inverse Shape Selectivity Revised. *Angew. Chem., Int. Ed.* **2002**, *41*, 2499−2502.
(20) Smit, B.; Maesen, T. L. M. Molecular Simulations of Zeolites: Adsorption, Diffusion, and Shape Selectivity. *Chem. Rev.* **2008**, *108*, 4125−4184.
(21) Smit, B.; Maesen, T. L. M. Towards a Molecular Understanding of Shape Selectivity. *Nature* **2008**, *451*, 671−678.
(22) Janda, A.; Vlaisavljevich, B.; Lin, L.-C.; Sharada, M. S.; Smit, B.; Head-Gordon, M.; Bell, A. T. Adsorption Thermodynamics and Intrinsic Activation Parameters for Monomolecular Cracking of N-Alkanes on Brønsted Acid Sites in Zeolites. *J. Phys. Chem. C* **2015**, *119*, 10427−10438.
(23) Swisher, J. A.; Hansen, N.; Maesen, T.; Keil, F. J.; Smit, B.; Bell, A. T. Theoretical Simulation of N-Alkane Cracking on Zeolites. *J. Phys. Chem. C* **2010**, *114*, 10229−10239.
(24) Van der Mynsbrugge, J.; Janda, A.; Mallikarjun Sharada, S.; Lin, L.-C.; Van Speybroeck, V.; Head-Gordon, M.; Bell, A. T. Theoretical Analysis of the Influence of Pore Geometry on Monomolecular Cracking and Dehydrogenation of N-Butane in Brønsted Acidic Zeolites. *ACS Catal.* **2017**, *7*, 2685−2697.
(25) Jiang, T.; Göltl, F.; Bulo, R. E.; Sautet, P. Effect of Temperature on the Adsorption of Short Alkanes in the Zeolite SSZ-13: Adapting Adsorption Isotherms to Microporous Materials. *ACS Catal.* **2014**, *4*, 2351−2358.
(26) Bučko, T.; Hafner, J. The Role of Spatial Constraints and Entropy in the Adsorption and Transformation of Hydrocarbons Catalyzed by Zeolites. *J. Catal.* **2015**, *329*, 32−48.
(27) Göltl, F.; Hafner, J. Modelling the Adsorption of Short Alkanes in Protonated Chabazite: The Impact of Dispersion Forces and Temperature. *Microporous Mesoporous Mater.* **2013**, *166*, 176−184.
(28) Janda, A.; Bell, A. T. Effects of Si/Al Ratio on the Distribution of Framework Al and on the Rates of Alkane Monomolecular Cracking and Dehydrogenation in H-MFI. *J. Am. Chem. Soc.* **2013**, *135*, 19193−19207.
(29) Sharada, S. M.; Zimmerman, P. M.; Bell, A. T.; Head-Gordon, M. Insights into the Kinetics of Cracking and Dehydrogenation Reactions of Light Alkanes in H-MFI. *J. Phys. Chem. C* **2013**, *117*, 12600−12611.
(30) Hunger, M. Brønsted Acid Sites in Zeolites Characterized by Multinuclear Solid-State NMR Spectroscopy. *Catal. Rev.: Sci. Eng.* **1997**, *39*, 345−393.
(31) Sarv, P.; Tuherm, T.; Lippmaa, E.; Keskinen, K.; Root, A. Mobility of the Acidic Proton in Broensted Sites of H-Y, H-Mordenite, and H-ZSM-5 Zeolites, Studied by High-Temperature 1H MAS NMR. *J. Phys. Chem.* **1995**, *99*, 13763−13768.
(32) Eder, F.; Stockenhuber, M.; Lercher, J. A. Brønsted Acid Site and Pore Controlled Siting of Alkane Sorption in Acidic Molecular Sieves. *J. Phys. Chem. B* **1997**, *101*, 5414−5419.
(33) Eder, F.; Lercher, J. A. On the Role of the Pore Size and Tortuosity for Sorption of Alkanes in Molecular Sieves. *J. Phys. Chem. B* **1997**, *101*, 1273−1278.
(34) Eder, F.; He, Y.; Nivarthy, G.; Lercher, J. A. Sorption of Alkanes on Novel Pillared Zeolites; Comparison between MCM-22 and MCM-36. *Recl. des Trav. Chim. des Pays-Bas* **1996**, *115*, 531−535.
(35) De Moor, B. A.; Reyniers, M.-F.; Gobin, O. C.; Lercher, J. A.; Marin, G. B. Adsorption of C2-C8 N-Alkanes in Zeolites. *J. Phys. Chem. C* **2011**, *115*, 1204−1219.
(36) International Zeolite Association http://www.iza-structure.org/databases/ (accessed Dec 28, 2017).
(37) Martin, M. G.; Siepmann, J. I. Transferable Potentials for Phase Equilibria. 1. United-Atom Description of N-Alkanes. *J. Phys. Chem. B* **1998**, *102*, 2569−2577.
(38) Dubbeldam, D.; Calero, S.; Vlugt, T. J. H.; Krishna, R.; Maesen, T. L. M.; Smit, B. United Atom Force Field for Alkanes in Nanoporous Materials. *J. Phys. Chem. B* **2004**, *108*, 12301−12313.
(39) Dubbeldam, D.; Calero, S.; Vlugt, T. J. H.; Krishna, R.; Maesen, T. L. M.; Beerdsen, E.; Smit, B. Force Field Parametrization through Fitting on Inflection Points in Isotherms. *Phys. Rev. Lett.* **2004**, *93*, 88302.
(40) Eder, F.; Lercher, J. A. Alkane Sorption in Molecular Sieves: The Contribution of Ordering, Intermolecular Interactions, and Sorption on Brønsted Acid Sites. *Zeolites* **1997**, *18*, 75−81.
(41) Barrer, R. M.; Davies, J. A. Sorption in Decationated Zeolites II. Simple Paraffins in H-Forms of Chabazite and Zeolite L. *Proc. R. Soc. London, Ser. A* **1971**, *322*, 1−19.
(42) Frenkel, D.; Smit, B. *Understanding Molecular Simulation: From Algorithms to Applications*, 2nd ed.; Academic Press: Cambridge, MA, 2001.
(43) Janda, A.; Vlaisavljevich, B.; Smit, B.; Lin, L.-C.; Bell, A. T. Effects of Pore and Cage Topology on the Thermodynamics of N-Alkane Adsorption at Brønsted Protons in Zeolites at High Temperature. *J. Phys. Chem. C* **2017**, *121*, 1618−1638.
(44) Tranca, D. C.; Hansen, N.; Swisher, J. A.; Smit, B.; Keil, F. J. Combined Density Functional Theory and Monte Carlo Analysis of Monomolecular Cracking of Light Alkanes Over H-ZSM-5. *J. Phys. Chem. C* **2012**, *116*, 23408−23417.
(45) Willems, T. F.; Rycroft, C. H.; Kazi, M.; Meza, J. C.; Haranczyk, M. Algorithms and Tools for High-Throughput Geometry-Based Analysis of Crystalline Porous Materials. *Microporous Mesoporous Mater.* **2012**, *149*, 134−141.
(46) Lowenstein, W. The Distribution of Aluminium in the Tetrahedra of Silicates and Aluminates. *Am. Mineral.* **1954**, *39*, 92−96.
(47) Rice, M. J.; Chakraborty, A. K.; Bell, A. T. Al Next Nearest Neighbor, Ring Occupation, and Proximity Statistics in ZSM-5. *J. Catal.* **1999**, *186*, 222−227.
(48) Han, O. H.; Kim, C.-S.; Hong, S. B. Direct Evidence for the Nonrandom Nature of Al Substitution in Zeolite ZSM-5: An Investigation by 27Al MAS and MQ MAS NMR. *Angew. Chem., Int. Ed.* **2002**, *41*, 469−472.
(49) Sklenak, S.; Dědeček, J.; Li, C.; Wichterlová, B.; Gábová, V.; Sierka, M.; Sauer, J. Aluminum Siting in Silicon-Rich Zeolite Frameworks: A Combined High-Resolution 27Al NMR Spectroscopy and Quantum Mechanics/Molecular Mechanics Study of ZSM-5. *Angew. Chem., Int. Ed.* **2007**, *46*, 7286−7289.
(50) Pinar, A. B.; Márquez-Álvarez, C.; Grande-Casas, M.; Pérez-Pariente, J. Template-Controlled Acidity and Catalytic Activity of Ferrierite Crystals. *J. Catal.* **2009**, *263*, 258−265.
(51) Han, O. H.; Kim, C.-S.; Hong, S. B. Direct Evidence for the Nonrandom Nature of Al Substitution in Zeolite ZSM-5: An Investigation by 27Al MAS and MQ MAS NMR. *Angew. Chem., Int. Ed.* **2002**, *41*, 469−472.
(52) Sklenak, S.; Dědeček, J.; Li, C.; Wichterlová, B.; Gábová, V.; Sierka, M.; Sauer, J. Aluminum Siting in Silicon-Rich Zeolite Frameworks: A Combined High-Resolution 27Al NMR Spectroscopy and Quantum Mechanics/Molecular Mechanics Study of ZSM-5. *Angew. Chem., Int. Ed.* **2007**, *46*, 7286−7289.
(53) Sklenak, S.; Dedecek, J.; Li, C.; Wichterlova, B.; Gabova, V.; Sierka, M.; Sauer, J. Aluminium Siting in the ZSM-5 Framework by Combination of High Resolution 27Al NMR and DFT/MM Calculations. *Phys. Chem. Chem. Phys.* **2009**, *11*, 1237−1247.

DOI: 10.1021/acs.jpcc.7b11190
J. Phys. Chem. C 2018, 122, 9397−9410

(54) Dedecek, J.; Lucero, M. J.; Li, C.; Gao, F.; Klein, P.; Urbanova, M.; Tvaruzkova, Z.; Sazama, P.; Sklenak, S. Complex Analysis of the Aluminum Siting in the Framework of Silicon-Rich Zeolites. A Case Study on Ferrierites. *J. Phys. Chem. C* **2011**, *115*, 11056−11064.
(55) Pinar, A. B.; Verel, R.; Pérez-Pariente, J.; van Bokhoven, J. A. Direct Evidence of the Effect of Synthesis Conditions on Aluminum Siting in Zeolite Ferrierite: A 27Al MQ MAS NMR Study. *Microporous Mesoporous Mater.* **2014**, *193*, 111−114.
(56) Pashkova, V.; Sklenak, S.; Klein, P.; Urbanova, M.; Dědeček, J. Location of Framework Al Atoms in the Channels of ZSM-5: Effect of the (Hydrothermal) Synthesis. *Chem. - Eur. J.* **2016**, *22*, 3937−3941.
(57) Dedecek, J.; Balgová, V.; Pashkova, V.; Klein, P.; Wichterlová, B. Synthesis of ZSM-5 Zeolites with Defined Distribution of Al Atoms in the Framework and Multinuclear MAS NMR Analysis of the Control of Al Distribution. *Chem. Mater.* **2012**, *24*, 3231−3239.
(58) Yokoi, T.; Mochizuki, H.; Namba, S.; Kondo, J. N.; Tatsumi, T. Control of the Al Distribution in the Framework of ZSM-5 Zeolite and Its Evaluation by Solid-State NMR Technique and Catalytic Properties. *J. Phys. Chem. C* **2015**, *119*, 15303−15315.
(59) Di Iorio, J. R.; Gounder, R. Controlling the Isolation and Pairing of Aluminum in Chabazite Zeolites Using Mixtures of Organic and Inorganic Structure-Directing Agents. *Chem. Mater.* **2016**, *28*, 2236−2247.
(60) Bernauer, M.; Tabor, E.; Pashkova, V.; Kaucký, D.; Sobalík, Z.; Wichterlová, B.; Dedecek, J. Proton Proximity − New Key Parameter Controlling Adsorption, Desorption and Activity in Propene Oligomerization over H-ZSM-5 Zeolites. *J. Catal.* **2016**, *344*, 157−172.
(61) Biligetu, T.; Wang, Y.; Nishitoba, T.; Otomo, R.; Park, S.; Mochizuki, H.; Kondo, J. N.; Tatsumi, T.; Yokoi, T. Al Distribution and Catalytic Performance of ZSM-5 Zeolites Synthesized with Various Alcohols. *J. Catal.* **2017**, *353*, 1−10.
(62) Ohio Supercomputer Center http://osc.edu/ark:/19495/f5s1ph73 (accessed Dec 28, 2017).

DOI: 10.1021/acs.jpcc.7b11190
J. Phys. Chem. C 2018, 122, 9397−9410